20th Australasian Fluid Mechanics Conference
Perth, Australia
5-8 December 2016

An External Line Plume next to a Dissolving Ice Face

C. D. McConnochie[1] and R. C. Kerr[1]

[1]Research School of Earth Sciences
The Australian National University, ACT 2601, Australia

Abstract

We present experiments that investigate the effect of a turbulent line plume next to a dissolving vertical ice face. The ice face provides a distributed source of buoyancy in addition to the buoyancy flux from the line plume at the base of the ice. The buoyancy flux, B_s is varied from $0.5B_o$ to $28B_o$ where B_o is the distributed buoyancy flux from the ice wall without the additional line plume. The plume velocity, ablation velocity of the ice and the temperature at the ice-fluid interface are measured over the height of the ice face. When B is small, the line plume is not dynamically important. However, as B increases the plume transitions to a regime where the distributed buoyancy flux from the ice wall is negligible and the line plume controls the flow. Within this regime the plume velocity is proportional to $B^{1/3}$ and the ablation velocity increases as B increases.

Introduction

Mass loss from the Antarctic and Greenland Ice Sheets is an important element of global sea level rise. The response of these ice sheets to a warmer climate is uncertain, making predictions of future sea level rise difficult. As such, a greater understanding of the processes occurring at the ice-ocean interface is needed to constrain possibilities of the future climate.

Laboratory experiments and theoretical analysis have been conducted that investigate the ablation velocity, interface temperature and plume properties when ice dissolves into homogeneous [4, 5] and stratified [6] salty water. In a homogeneous ambient fluid, it was found that the ablation rate and interface temperature are uniform with height and that the plume velocity increases like $z^{1/3}$. Stratification acts to reduce the ablation rate, the interface temperature and the plume velocity.

Subglacial plumes have been observed at a variety of outlet glaciers around Greenland and are almost always associated with high ablation rates [2]. The plumes are typically assumed to have zero salinity and be at the pressure dependent freezing point. In one particular fjord, the volume flux of the subglacial plume discharged at the base of two typical Greenland glaciers was estimated to be roughly four times the meltwater volume flux in the region of the plume [1].

A number of numerical modelling studies have investigated the effect of these subglacial plumes on ice-ocean interactions. A recent review of these studies suggests that "the submarine melt rate increases with increasing subglacial discharge (with a power of 1/3), linearly increases with increasing temperature, and increases with vertical distance above the grounding line in winter and slightly decreases with it in summer [12]."

This paper presents experiments that investigate the effect of a turbulent two-dimensional subglacial plume on the ice ablation rate, the interface temperature and the plume velocity. In particular, we examine the behaviour as the plume transitions from being dominated by the distributed buoyancy flux due to dissolution to being dominated by the external source of buoyancy at the base of the ice.

Scaling

Our experiments lie between two limiting cases. These can be described by a non-dimensional parameter, B^*, defined as:

$$B^* = \frac{B_s + B_o}{B_o} \tag{1}$$

where B_s is the imposed buoyancy flux from the freshwater source and B_o is the buoyancy flux that would be expected from the ice wall without an external plume [4].

When $B_s = 0$, there is no imposed buoyancy flux and $B^* = 1$. This represents the wall plume from a distributed source of buoyancy [5]. Alternatively, when $B_s \gg B_o$, B^* will be large and the distributed buoyancy flux from the wall will be negligible. Here the plume can be described as a wall plume from a line source of buoyancy at the base of the wall.

The wall plume from a distributed source of buoyancy can be described by the following model :

$$\begin{aligned} b_T &= 0.036z, & w_T &= 1.2\Phi^{1/3}z^{1/3} \\ \Delta_T &= 23\Phi^{2/3}z^{-1/3}, & Q &= 0.043\Phi^{1/3}z^{4/3} \end{aligned} \tag{2}$$

where b_T is the top-hat plume width, w_T is the top-hat plume velocity, Δ_T is the top-hat plume buoyancy, Q is the plume volume flux, z is the height above a virtual source and Φ is the buoyancy flux per unit area [5].

Equation 2 can be contrasted with a model of a line plume next to a wall:

$$\begin{aligned} b_T &= \alpha z, & w_T &= \left(\frac{B_s}{\alpha + c_D}\right)^{1/3} \\ \Delta_T &= \frac{B_s^{2/3}(\alpha + c_D)^{1/3}}{\alpha z}, & Q &= b_T w_T = \frac{\alpha B_s^{1/3} z}{(\alpha + c_D)^{1/3}} \end{aligned} \tag{3}$$

where α is the entrainment coefficient and c_D is the drag coefficient. Estimates of the drag coefficient [13, 3] are typically an order of magnitude smaller than the entrainment coefficient [9], allowing c_D to be neglected in equation 3.

Experiments

Experiments have been conducted to examine the effect of a cold freshwater line plume next to a vertical ice face. The experiments were carried out in a tank that was 1.2 m high, 1.5 m long and 0.2 m wide, with an overflow 1.1 m from the base. Figure 1 shows a photo from an experiment with $B^* = 21.2$ that has been visualized using the shadowgraph technique. Ice can be seen on the right of the image and the quiescent ambient fluid on the left. The external plume was seen to attach to the ice face as it is released. For experiments performed at lower values of B^* the transition to turbulence was further up the ice wall but never as much as 10 cm from the source location.

Table 1 gives the experimental parameters and computed values of B^*. For some of the low flow rate experiments, the source

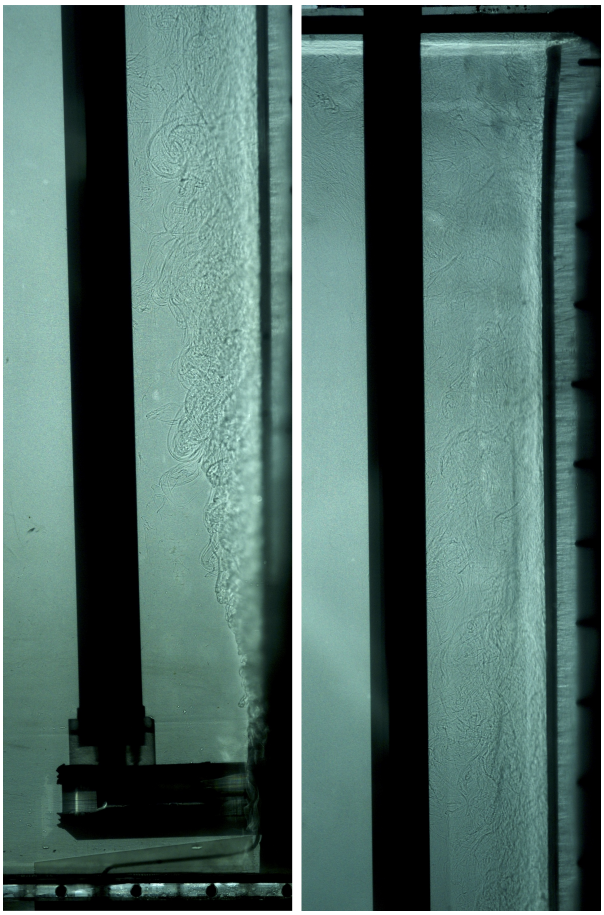

Figure 1: A shadowgraph image of an experiment with $B^* = 21.2$. The ice can be seen on the right hand side of the image and the quiescent ambient fluid on the left. Immediately next to the ice the turbulent wall plume can be seen. The left image shows the base of the tank up to a height of 59 cm and the right image shows a height of 49 cm to the free surface at 110 cm.

temperature was not as cold as desired due to heat transfer between the reservoir and the source. However, the plume was observed to rapidly entrain ambient fluid so the effect of this should be minimal apart from very close to the source.

Throughout an experiment the ablation velocity and interface temperature were measured as described in previous experiments [4]. Thermistors were frozen into the ice at heights of 43 cm, 50 cm, 55 cm and 68 cm above the base of the tank. A second thermistor was positioned 68 cm above the base of the tank to confirm that there was no horizontal variation in interface temperature.

The plume velocity was measured using the Particle Tracking Velocimetry (PTV) technique. Pliolite particles of diameter $125-250\,\mu$m were seeded into the ambient fluid and were then entrained into the line plume. The particles had a calculated rise velocity of 0.03 mm/s to 0.12 mm/s in the ambient fluid depending on the particle size. This particle rise velocity is negligible compared to typical plume velocities, which vary from 14 mm/s at the lowest source flow rates to 37 mm/s at the highest source flow rate.

B^* -	T_f (°C)	C_f (wt% NaCl)	Q_s (ml/s)	T_s (°C)
1.0	3.8	3.46	0.0	-
1.6	3.5	3.50	0.3	1.8
2.2	3.5	3.52	0.6	1.5
3.3	3.6	3.51	1.2	1.3
3.7	3.7	3.46	1.4	1.1
6.1	3.6	3.54	2.6	0.9
6.3	4.1	3.47	2.8	0.8
7.2	3.8	3.45	3.2	0.8
7.6	3.5	3.64	3.4	0.9
10.6	3.9	3.44	5.0	0.6
18.8	4.7	3.49	9.3	0.3
27.0	4.2	3.50	13.5	0.3
29.3	3.6	3.52	14.7	0.1
33.1	4.5	3.38	16.7	0.1

Table 1: Experimental parameters for all experiments. All results are reported in terms of the non-dimensionalised buoyancy flux, B^*. T_f and C_f are the far-field fluid temperature and salinity respectively. Q_s is the source volume flux and T_s is the source temperature.

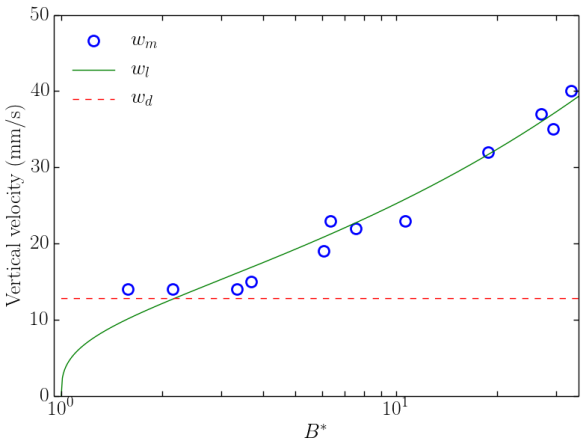

Figure 2: Measured maximum vertical velocity as a function of B^*. The dashed and solid lines show the predicted velocity based on equations 2 and 3 respectively.

Results

Plume Velocity

For sufficiently large values of B^* the plume velocity is observed to reach a constant value as predicted by equation 3. Figure 2 shows the measured maximum vertical velocity, w_m, as a function of B^* as well as the predicted vertical velocity, w_l from the model of a wall plume from a line source of buoyancy (equation 3) and the predicted velocity, w_d from the model of a wall plume from a distributed source of buoyancy (equation 2). w_m is measured after the velocity has approached a uniform value with height when possible and at a height of around 0.8 m elsewhere. In calculating w_l the drag coefficient is assumed to be negligible and an entrainment coefficient of 0.075 is used based on the experimental data.

Figure 2 shows that for $B^* < 2$ the distributed buoyancy source from the ice wall has an important effect on the plume velocity but can be ignored for larger values of B^*. For $B^* > 2$ the model of a wall plume from a line source of buoyancy described in equation 3 accurately predicts the plume velocity with an entrainment coefficient of 0.075.

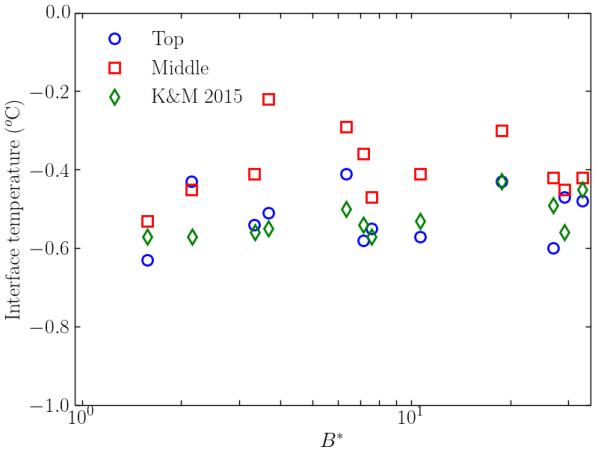

Figure 3: Measured interface temperature, T_i, as a function of B^*.

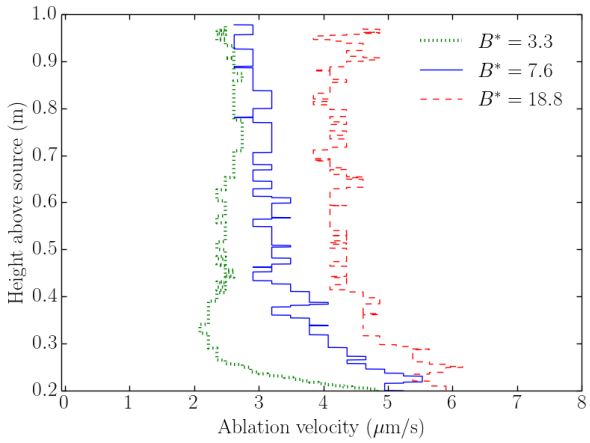

Figure 4: Measured ablation velocity as a function of height above the source for three typical experiments.

Interface Temperature

Figure 3 shows the interface temperature at two locations up the ice wall: "top" and "middle". These two locations reflect thermistor locations of 0.68 m and 0.43 – 0.50 m from the base of the tank respectively. The typical difference between the two thermistors positioned 0.68 m above the base of the tank was used to assess a measurement uncertainty of $\pm$ 0.1 °C which is reflected in the scatter of the data points. The interface temperature measured for a wall plume from a distributed source of buoyancy is shown with green diamonds [4]. The variation between experiments is due to changes in the far field fluid temperature.

The interface temperature at both measurement locations is constant within experimental error over the full range of B^*. The interface temperature is slightly higher in the middle region than at the top region suggesting the presence of a transition zone.

Ablation Velocity

Figure 4 shows the measured ablation velocity as a function of height above the source for three experiments with $B^* = 3.3$, 7.6, and 18.8. Throughout most of the tank the ablation velocity is near-uniform with height as observed for the case of a distributed source of buoyancy ($B^* = 1$) [4].

Figure 5 shows the measured ablation anomaly as a function

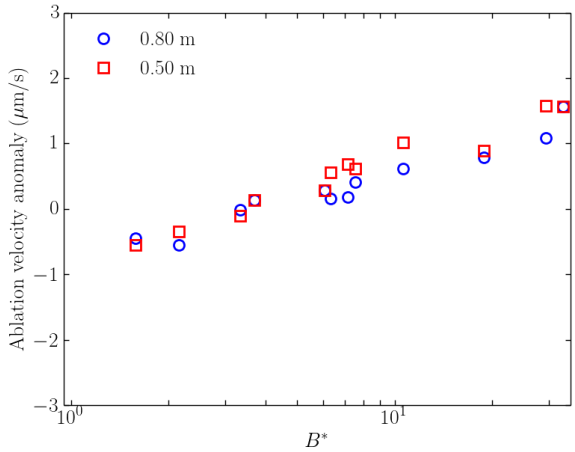

Figure 5: The ablation anomaly cuased by the source plume as a function of B^*.

of B^*. The ablation anomaly is calculated by subtracting the predicted ablation velocity for a distributed buoyancy source [4] from the observed ablation velocity. This shows the enhanced ablation caused by the source plume without any effect caused by changes in the ambient fluid temperature or salinity. For comparison, the predicted ablation velocity is typically around $2.5 - 3$ μm/s [4].

Figure 5 shows that the ablation velocity generally increases smoothly with B^*. For $B^* < 3$ the ablation velocity appears to be decreased by the presence of a source plume. The reduction in ablation velocity is larger than the measurement uncertainty so is not expected to be caused by experimental error. The line source of buoyancy introduces a salinity and temperature deficit to the wall plume. For high values of B^*, the initial temperature and salinity deficit quickly decays due to turbulent entrainment of ambient fluid into the plume. However, at low values of B^*, the wall plume is dominated by the distributed source of buoyancy rather than the line source of buoyancy. The wall plume from a distributed source of buoyancy has a lower rate of entrainment which could allow the salinity and temperature deficit to persist up the ice wall and lead to a reduced ablation rate. For $B^* > 3$ the ablation velocity anomaly is positive and increases with increasing B^*.

Oceanographic Application

Table 2 gives estimated values of B^* for a variety of tidewater glaciers. Two different methods have been used to calculate B^*. For Byrd Glacier, Helheim Glacier, LeConte Glacier and Store Glacier, the subglacial discharge and the width over which it is released has been directly estimated [7, 10, 11, 14]. This has been combined with an assumed ablation velocity of 3 μm/s in order to estimate B^*. For Eqip Sermia, Kangerlerngata Sermia, Sermeq Kujatdleq and Sermeq Avangnandleq the ratio of subglacial volume flux to meltwater volume flux was inferred based on measured water properties in front of the glacier [1, 8]. This ratio of fluxes was used to directly calculate B^* based on the assumption that the subglacial discharge was released uniformly over the entire width of the glacier. If the subglacial discharge was released from a more limited width [2], the resulting value of B^* would be higher in regions where the subglacial flux per unit width was larger and lower elsewhere.

Over the seven locations in table 2, B^* varies from an order of 10^0 – 10^3. Most of the glaciers have a value of B^* that is comparable to our experiments with the exceptions of LeConte Glacier and Store Glacier. The values of B^* given in table 2

Location -	H (m)	W (m)	Q_{sg} (m^3/s)	B^* -
Byrd Glacier, Antarctica [11]	700	20000	70	3
Helheim Glacier, Greenland [10]	600	200	8.7	31
	600	6000	0.29	1.03
LeConte Glacier, Alaska [7]	270	700	435	950
Store Glacier, Greenland [14]	500	5000	1500	249
Eqip Sermia, Greenland [1]				6
Eqip Sermia, Greenland [8]				19
Kangerlerngata Sermia, Greenland [1]				6
Kangerlerngata Sermia, Greenland [8]				29
Sermeq Kujatdleq and Sermeq Avangnandleq, Greenland [8]				4

Table 2: Estimated values of glacier height, H, subglacial discharge width, W, subglacial volume flux, Q_{sg}, and B^* for a variety of tidewater glaciers. Observations for Byrd Glacier were made during a sporadic subglacial lake drainage event while other observations are representative of summer conditions.

for Alaskan and Greenlandic glaciers are representative of summer conditions only and are expected to be highly seasonal. In winter the subglacial volume flux will decrease and probably stop completely. At such times $B^* \approx 1$, the ablation velocity will be as described by theory based on a distributed buoyancy source [4] and the plume velocity will be as described by equation 2. In the case of Byrd Glacier, the measured subglacial discharge was caused by the rapid draining of a subglacial lake and was highly unusual. The hydrology beneath the Antarctic ice sheet is not well understood but such events are rarely observed. As such, typical ablation velocities and plume velocities for Antarctic glaciers would be typically described by $B^* \approx 1$.

Conclusions

In this paper we have presented experiments that investigate the effect of an external cold freshwater plume on the dissolution of a vertical ice face. These experiments are intended to model conditions at the face of the many Greenland glaciers where subglacial plumes are observed during summer months. The experiments have explored a range of source volume fluxes that bridge the region between a wall plume controlled by a vertically distributed buoyancy source and a wall plume controlled by a line source of buoyancy at the base of a wall.

Our results generally show that an additional line source of buoyancy causes the plume velocity to increase (figure 2) and the ablation velocity to increase (figure 5) relative to the case of a wall plume from a distributed source of buoyancy [4, 5]. For small buoyancy fluxes ($B^* < 3$) the ablation velocity is slightly reduced. The interface temperature appears to be insensitive to the line source of buoyancy (figure 3).

Acknowledgements

We gratefully acknowledge the technical assistance of Ben Tranter, Tony Beasley and Angus Rummery, and the financial support of the Australian Research Council Discovery Grant DP120102772.

References

[1] Beaird, N., Straneo, F. and Jenkins, W., Spreading of Greenland meltwaters in the ocean revealed by noble gases, *Geophys. Res. Lett.*, **42**, 2015, 7705-7713.

[2] Fried, M.J., Catania, G.A., Bartholomaus, T.C., Duncan, D., Davis, M., Stearns, L.A., Nash, J., Shroyer, E. and Sutherland, D., Distributed subglacial discharge drives significant submarine melt at a Greenland tidewater glacier, *Geophys. Res. Lett.*, **42**, 2015, 9328-9336.

[3] Jenkins, A., Convection-driven melting near the grounding lines of ice shelves and tidewater glaciers, *J. Phys. Oceanog.*, **41**, 2011, 2279-2294.

[4] Kerr, R.C. and McConnochie, C.D., Dissolution of a vertical solid surface by turbulent compositional convection, *J. Fluid Mech.*, **765**, 2015, 211-228.

[5] McConnochie, C.D. and Kerr, R.C., The turbulent wall plume from a vertically distributed source of buoyancy, *J. Fluid Mech.*, **787**, 2016, 237-253.

[6] McConnochie, C.D. and Kerr, R.C., The effect of a salinity gradient on the dissolution of a vertical ice face, *J. Fluid Mech.*, **791**, 2016, 589-607.

[7] Motyka, R.J., Hunter, L., Echelmeyer, K.A. and Connor, C., Submarine melting at the terminus of a temperature tidewater glacier, LeConte Glacier, Alaska, U.S.A., *Ann. Glaciol*, **36**, 2003, 57-65.

[8] Rignot, E., Koppes, M. and Velicogna, I., Rapid submarine melting of the calving faces of West Greenland glaciers, *Nature Geosci.*, **3**, 2010, 187-191.

[9] Sangras, R., Dai, Z. and Faeth, G.M., Mixture fraction statistics of plane self-preserving buoyant turbulent adiabatic wall plumes, *J. Heat Transfer*, **121**, 1999, 837-843.

[10] Sciascia, R., Straneo, F., Cenedese, C. and Heimbach, P., Seasonal variability of submarine melt rate and circulation in an East Greenland fjord, *J. Geophys. Res. Oceans*, **118**, 2013, 2492-2506.

[11] Stearns, L.A., Smith, B.E. and Hamilton, G.S., Increased flow speed on a large East Antarctic outlet glacier caused by subglacial floods, *Nature Geosci.*, **1**, 2008, 827-831.

[12] Straneo, F. and Cenedese, C, The dyanmics of Greenland's glacial fjords and their role in climate, *Annu Rev. Mar. Sci.*, **7**, 2015, 89-112.

[13] Wells, A.J. and Worster, M.G, A geophysical-scale model of vertical natural convection boundary layers, *J. Fluid Mech.*, **609**, 2008, 111-137.

[14] Xu, Y., Rignot, E., Fenty, I. and Menemenlis, D., Subaqueous melting of Store Glacier, West Greenland from three-dimensional, high resolution numerical modeling and ocean observations, *Geophys. Res. Lett.*, **40**, 2013, 4648-4653.